Supplemental material for "2010-2015 methane trends over Canada, the United States, and Mexico observed by the GOSAT satellite: contributions from different source sectors"

Jian-Xiong Sheng, Daniel J. Jacob, Alexander J. Turner, Joannes D. Maasakkers, Joshua Benmergui, A. Anthony Bloom, Claudia Arndt, Ritesh Gautam, Daniel Zavala-Araiza, Hartmut Boesch, Robert J. Parker

Contents

1 GOSAT seasonal coverage bias in North America

The total number of GOSAT retrievals in the winter in Canada ranges from 350 to 500 for 2010-2015, as compared to 700-1200 in the summer. Figure S1 shows the 2015 GOSAT retrieval density in North America for the winter months and for the whole year. There are less retrievals in the wintertime in high latitudes. This demonstrates the seasonal bias in the sampling of GOSAT that mainly affects high latitudes (north of 45°). GOSAT data is from the version 7.0 proxy methane retrievals in the high-gain nadir modes (Parker et al., 2011).

2 Permutation resampling tests for low quantiles

We use a permutation resampling method to test the null hypothesis that the low percentiles as background of GOSAT observations for a given location and year are statistically not different from instrument error. Under this null hypothesis, permuting the local background would have no effect on the total enhancement Δ (see Eq. (1) in the main text) for a given region, when variation due to surface elevation and tropopause height is taken into account. Figure S2 shows as an example three permutation distributions of the total enhancements Δ for CONUS in 2015 derived from a random sample of 10,000 permutations of the 1st, 10th, and 20th percentiles as local background. The observed Δ using the 1st percentiles as local background can be well explained by variation of the permutation distribution (within 1σ) , thus the null hypothesis cannot be rejected. The observed Δ using the 10th percentiles or above as local background is at the left far-end tail ($|\text{standard z-score}| > 2$) and unlikely from the permutation distribution, and thus we may reject the null hypothesis.

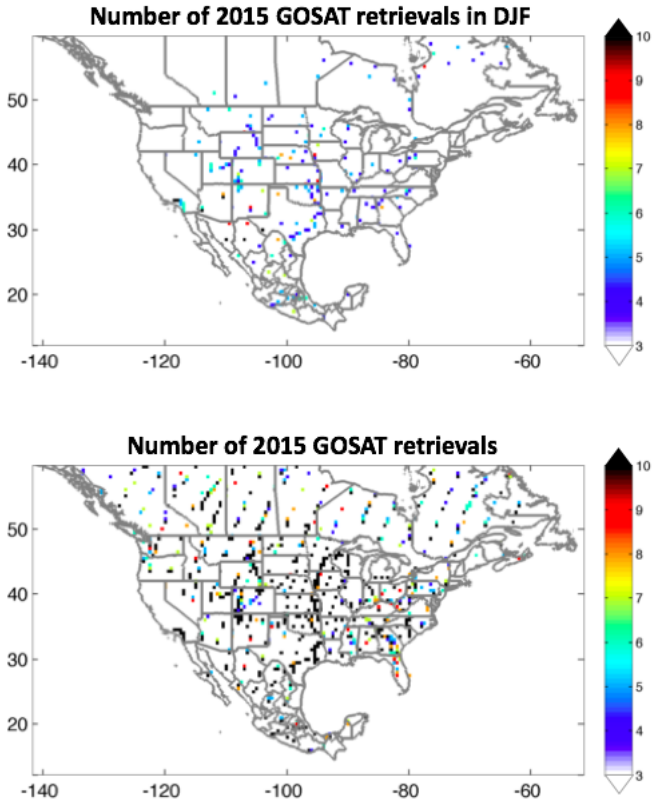

Figure S1: GOSAT retrieval density in North America in 2015

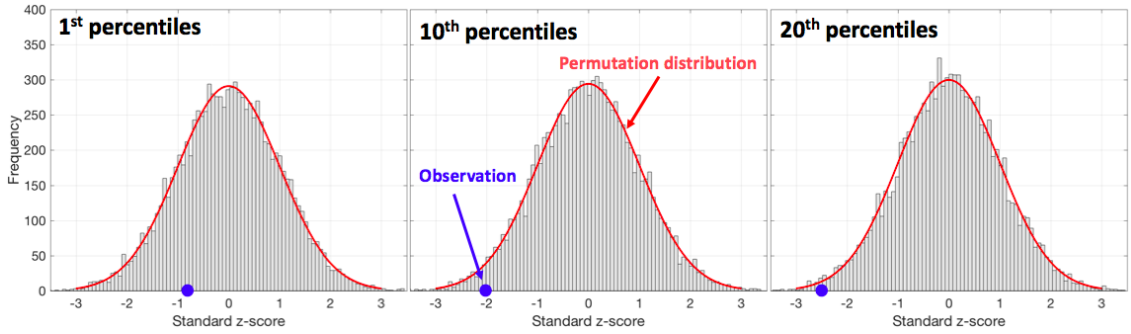

Figure S2: Permutation distributions of the total enhancements Δ for CONUS using the 1st, 10th, and 20th percentiles as local background under the null hypothesis that the low percentiles are statistically not different from instrumental noises. Standard z-score $z = \frac{\Delta - \overline{\Delta}}{\sigma}$ with the mean ($\overline{\Delta}$) and standard deviation (σ) of the permutation distribution.

3 Wetland-dominated areas

Figure S3 shows the locations of high-emitting $0.5^\circ \times 0.5^\circ$ grid cells dominated by different sectors as informed by the bottom-up inventories of Section 2 in the main text. Wetland-dominated areas in the upper panel are identified by the mean of model runs (Bern, CLM4Me, DLEM, ORCHIDEE, WSL) that cover North America from WETCHIMP (Melton et al., 2013) . Wetland-dominated areas in the lower panel are identified by the WetCHARTs mean inventory (Bloom et al., 2017). We use their common areas to define wetland high-emitting grid cells, as shown in Fig. 4 in the main text.

4 Spatial distribution of GOSAT methane trends in North America

Figure S4 shows the spatial distribution of 2010-2015 GOSAT methane trends in local enhancements in North America at $4^\circ \times 4^\circ$ spatial resolution from January 2010 to December 2015 (six years). The trends are inferred from linear regression of the enhancements for individual years. There is a general pattern of increase in the US and decrease in Mexico. However, the trends are generally not significant.

5 Probability density of year-to-year variability in methane enhancements

Figure S5 shows the probability density of the 2015 change (%) in the total enhancement Δ (see Eq.(1) in the main text) over CONUS relative to 2010. The density function is constructed by 1000 Monte Carlo realizations where the background for each grid cell and year is obtained by random sampling of percentiles in the 10th-25th (black), 10th-20th (red), and 15th-20th (blue) ranges.

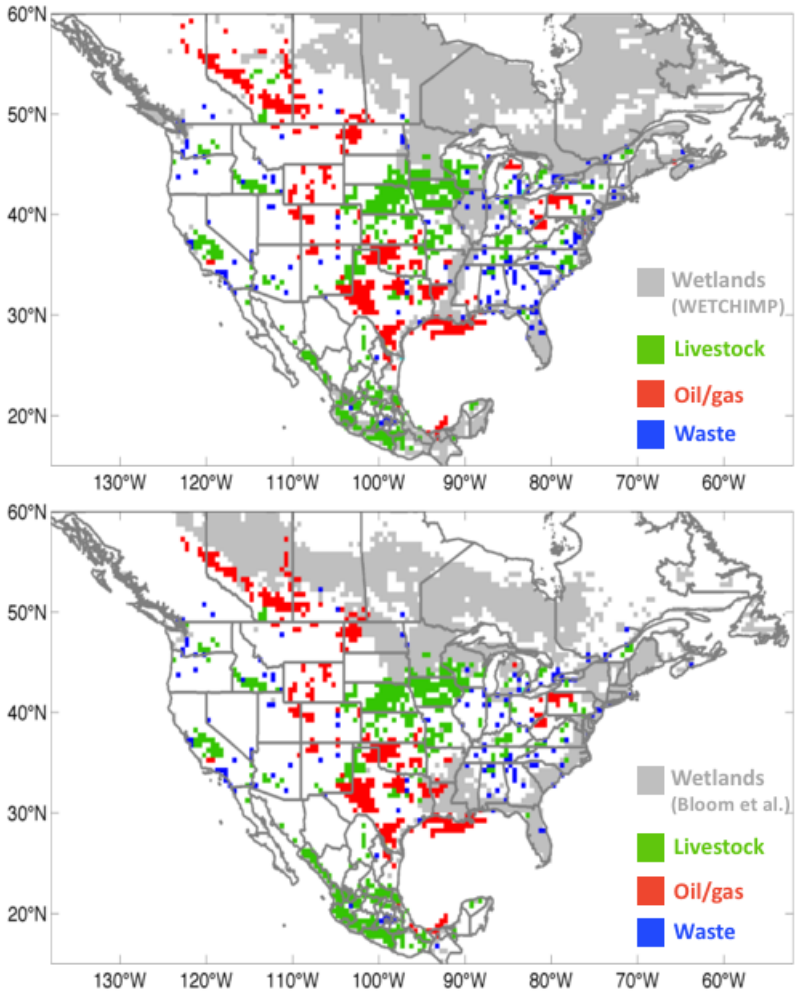

Figure S3: High methane emissions in North America dominated by a particular sector as identified by the bottom-up inventories (see main text for details). High-emitting wetland areas are identified by the WETCHIMP mean (upper panel) and by the WetCHARTs inventories (lower panel).

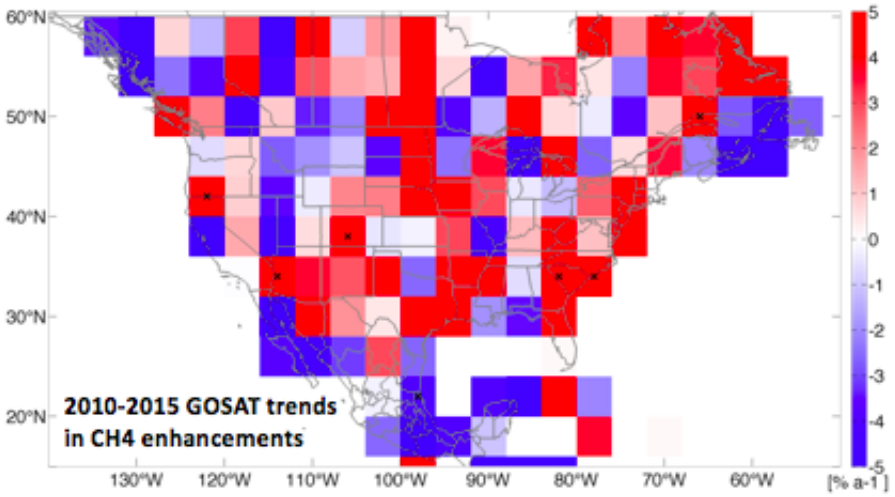

Figure S4: 2010-2015 trends in GOSAT methane enhancements over North America as metric for changes in methane emissions for $4° \times 4°$ grid cells, where methane enhancements are defined relative to a local low-quantile background as described in the main text. Crosses indicate significant trends at the 0.05 level.

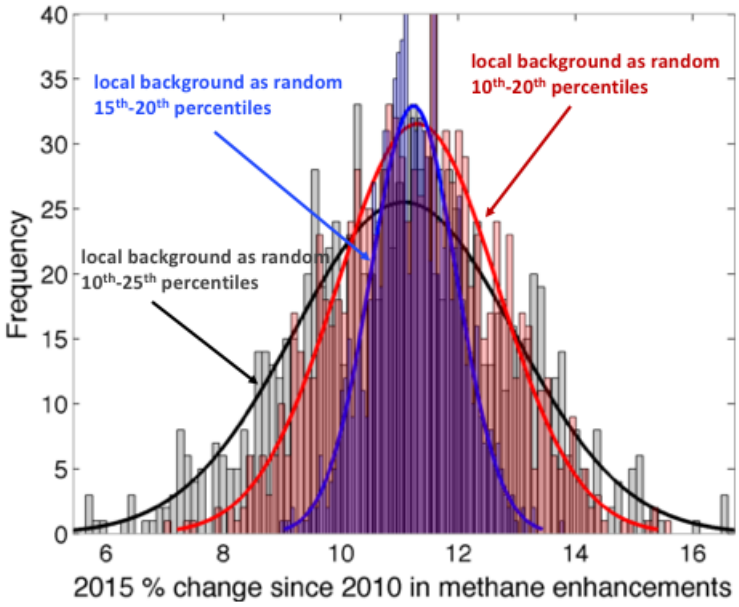

Figure S5: Frequency distribution of 2015 change (%) since 2010 for the total CH_4 enhancement over CONUS.

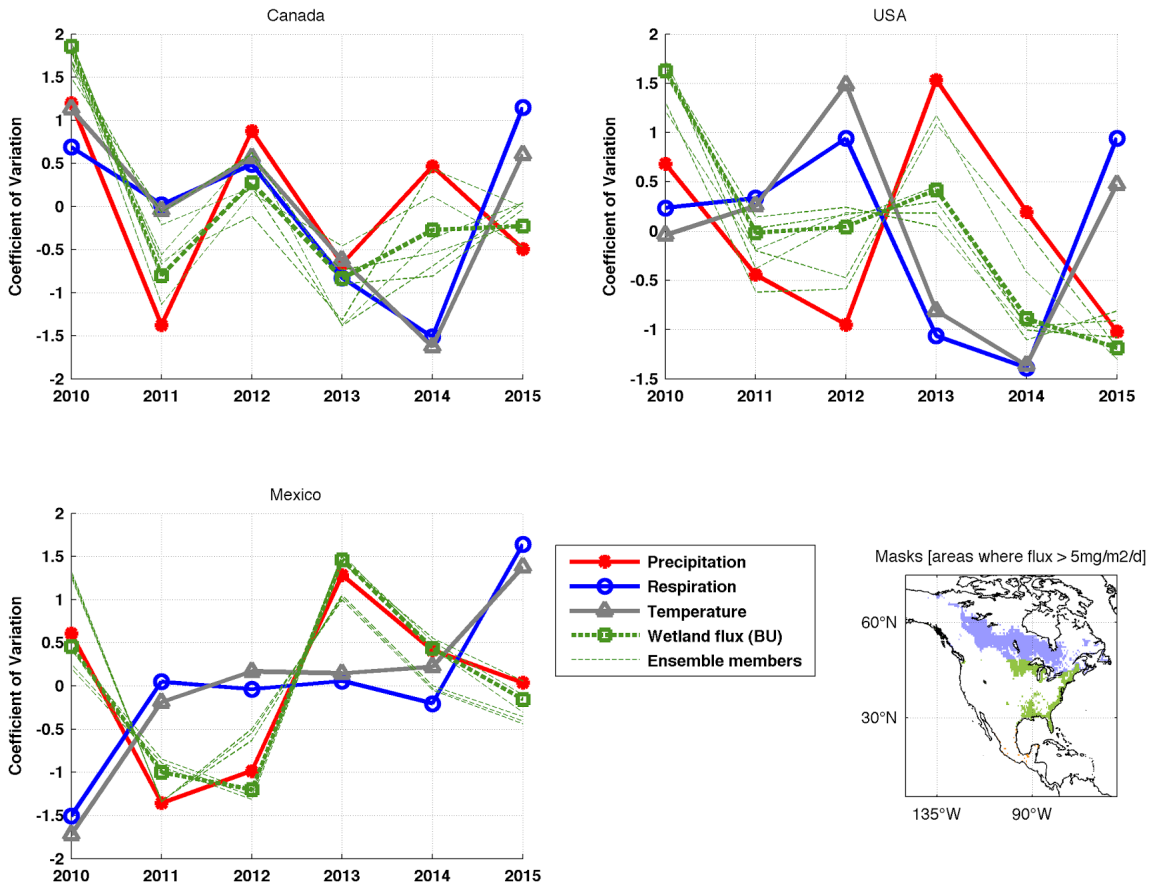

Figure S6: The annual means for the wetland CH_4 controls for 2010-2015.

6 Wetlands controls

Figure S6 shows the annual means for the wetland CH_4 controls (temperature, precipitation and carbon respiration) for 2010-2015 over Canada, CONUS, and Mexico used in the WetCHARTs wetland CH4 emission dataset (Bloom et al., 2017). Precipitation is assumed to be a proxy for wetland extent (Bloom et al., 2017). These control indices are within high-emitting wetland CH_4 emission areas.

7 Wind speed

Figure S7 shows the 2010-2015 time series of monthly mean 10-meter wind speeds averaged over the high-emitting grid cells dominated by different source sectors. Wind speeds are from NASA/GMAO MERRA-2 reanalysis data (`https://gmao.gsfc.nasa.gov/reanalysis/MERRA-2/`). The averaged wind speeds show no significant trends over 2010-2015 as indicated by the corresponding p-values.

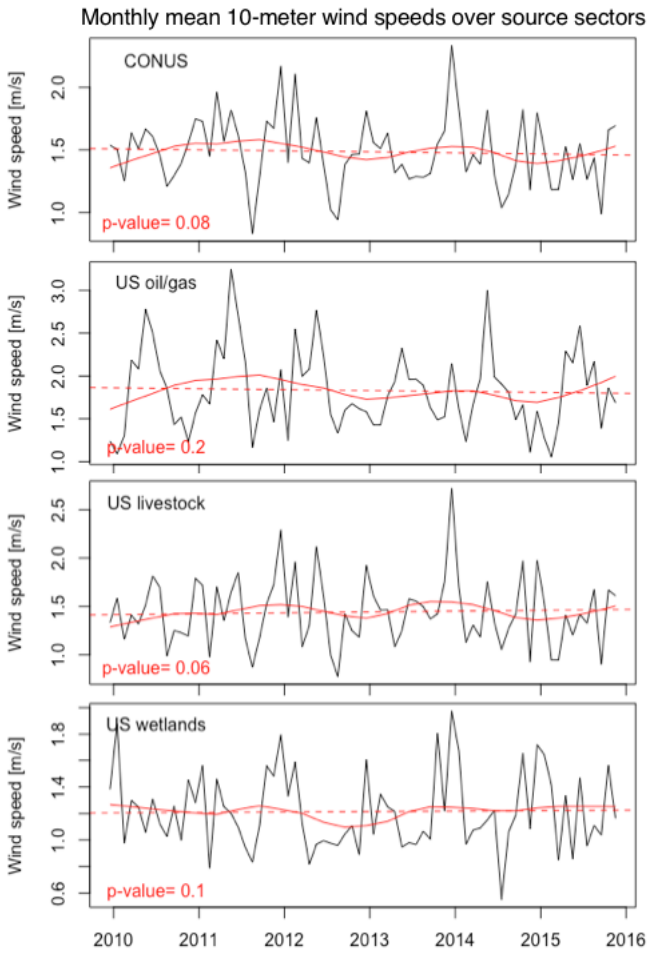

Figure S7: Time series of monthly mean 10-meter wind speeds averaged over the CONUS and high-emitting grid cells dominated by oil/gas, livestock, and wetlands in the US. Also shown are the moving averages (red, derived from STL decomposition method (Cleveland et al., 1990)) and the corresponding p-values of their linear trends.

References

A. A. Bloom, K. Bowman, M. Lee, A. J. Turner, R. Schroeder, J. R. Worden, R. Weidner, K. C. McDonald, and D. J. Jacob. A global wetland methane emissions and uncertainty dataset for atmospheric chemical transport models. *Geoscientific Model Development*, pages 1–37, 2017. ISSN 1991-959X. doi: 10.5194/gmd-2016-224. URL `http://www.geosci-model-dev-discuss.net/gmd-2016-224/`.

R. B. Cleveland, W. S. Cleveland, and I. Terpenning. STL: A seasonal-trend decomposition procedure based on loess. *Journal of Official Statistics*, 6(1):3, 1990.

J. R. Melton, R. Wania, E. L. Hodson, B. Poulter, B. Ringeval, R. Spahni, T. Bohn, C. A. Avis, D. J. Beerling, G. Chen, A. V. Eliseev, S. N. Denisov, P. O. Hopcroft, D. P. Lettenmaier, W. J. Riley, J. S. Singarayer, Z. M. Subin, H. Tian, S. Zrcher, V. Brovkin, P. M. van Bodegom, T. Kleinen, Z. C. Yu, and J. O. Kaplan. Present state of global wetland extent and wetland methane modelling: conclusions from a model inter-comparison project (WETCHIMP). *Biogeosciences*, 10 (2):753–788, Feb. 2013. ISSN 1726-4189. doi: 10.5194/bg-10-753-2013. URL `http://www.biogeosciences.net/10/753/2013/`.

R. Parker, H. Boesch, A. Cogan, A. Fraser, L. Feng, P. I. Palmer, J. Messerschmidt, N. Deutscher, D. W. T. Griffith, J. Notholt, P. O. Wennberg, and D. Wunch. Methane observations from the Greenhouse Gases Observing SATellite: Comparison to ground-based TCCON data and model calculations. *Geophys. Res. Lett.*, 38(15):L15807, Aug. 2011. ISSN 1944-8007. doi: 10.1029/2011GL047871. URL `http://onlinelibrary.wiley.com/doi/10.1029/2011GL047871/abstract`.